Synthesis, characterization and physical properties of the skutterudites YbxFe2Ni2Sb12 (0x0.4)

Synthesis, Characterization and Physical Properties of the Skutterudites $Yb_xFe_2Ni_2Sb_{12}$ ($0 \leq x \leq 0.4$)

Andreas Kaltzoglou[a], Paz Vaqueiro[a], Kevin S. Knight[b], Anthony V. Powell[a,*]

[a] *Department of Chemistry, Heriot-Watt University, Edinburgh EH14 4AS, UK*

[b] *ISIS Facility, Rutherford Appleton Laboratory, Didcot, Oxfordshire OX11 0OX, UK*

* Corresponding author. Fax: +44(0)-131-4513180
E-mail: a.v.powell@hw.ac.uk

Abstract

The skutterudites $Yb_xFe_2Ni_2Sb_{12}$ ($0 \leq x \leq 0.4$) have been prepared by solid-state reaction and characterized by powder X-ray diffraction. The compounds crystallize in the cubic space group $Im\,\overline{3}$ ($a \approx 9.1$ Å) with Yb atoms partially filling the voids in the skutterudite framework. A neutron time-of-flight diffraction experiment for $Fe_2Ni_2Sb_{12}$ confirms the disorder of Fe and Ni atoms on the transition-metal site. Electrical resistivity, Seebeck coefficient and thermal conductivity measurements indicate that the thermoelectric performance of the skutterudites shows a marked dependence on the Yb content. Magnetic measurements over the temperature range $2 \leq T / \mathrm{K} \leq 300$ show paramagnetic behaviour for all compounds. Decomposition studies under oxidizing atmosphere at elevated temperatures have also been carried out by thermogravimetric analysis.

Keywords: Skutterudite; Thermoelectric Properties; Magnetic Properties, Diffraction

1. Introduction

The ideal skutterudite structure [1] consists of an array of vertex-linked metal centred MX_6 octahedra, which results in a framework of stoichiometry MX_3 (Figure 1). Octahedra are tilted according to the $a^+a^+a^+$ tilt system [2], generating large voids within the structure. The anion sub-lattice forms four-membered rectangular rings, which are believed to play a key role in determining the electronic properties [3]. Binary skutterudites MX_3 are known for M = Co, Rh, Ir; X = P, As, Sb. Moreover the large voids created within the framework may be occupied to varying degrees by filler atoms giving rise to filled skutterudites of general formula, $A_xM_4X_{12}$, where A may be a rare-earth, alkali metal, alkaline earth or group 13 element [4,5]. Filled skutterudites have been extensively studied as promising candidates for thermoelectric applications [6,7]. It has been suggested that such materials are manifestations of the 'phonon-glass and electron-crystal' concept (PGEC) proposed by Slack [8]. The guest atoms within the void space exhibit localized vibrational modes [9], known as rattling vibrations. These localized vibrations perturb the propagation of phonons, thereby significantly reducing the phonon contribution to the thermal conductivity. The PGEC concept postulates that this may occur without a degradation of the electrical properties of the material, which are primarily determined by the characteristics of the framework. It has been established that the properties of filled skutterudites can be tuned by varying the degree of filling of the voids with electropositive elements and through chemical substitution within the framework. The latter can also lead to charge compensation. Filled skutterudites have some of the highest thermoelectric figures of merit ($ZT = S^2T/\kappa\rho$, where S is the Seebeck coefficient, ρ the electrical resistivity and κ the thermal conductivity) at elevated temperatures, for example n-type $Ba_{0.30}Ni_{0.05}Co_{3.95}Sb_{12}$ ($ZT \approx 1.25$ at 900 K) [10] and p-type $Ce_{0.9}Fe_3CoSb_{12}$ ($ZT \approx 1.1$ at 700 K) [11].

The majority of studies of filled skutterudites have focused on the $CoSb_3$ framework [5]. By contrast, more limited investigations have been carried out for the analogous Fe/Ni phases.

Replacement of cobalt by equimolar amounts of iron and nickel, yields a ternary skutterudite that is isoelectronic with the binary cobalt antimonide. $Fe_2Ni_2Sb_{12}$ exhibits lower thermoelectric performance than Co_4Sb_{12}. Rare-earth-filled $Pr_{0.1}Fe_2Ni_2Sb_{12}$ [12] and $(Pr,Nd)_{0.08}Fe_2Ni_2Sb_{12}$ [13] have been reported to exhibit *n*-type behavior and a moderate thermoelectric response (*e.g.* $ZT \approx 0.4$ at 800 K for $(Pr,Nd)_{0.08}Fe_2Ni_2Sb_{12}$). A change to *p*-type behaviour may be induced by varying the Fe/Ni ratio as occurs in $(Ln)_x(Fe,Ni)_4Sb_{12}$ (*Ln* = Ce and/or Yb, $0 \leq x \leq 0.95$) [14]. Theoretical calculations on alkaline-earth-filled skutterudites $Ae(Fe,Ni)_4Sb_{12}$ (*Ae* = Ca, Sr, Ba) predict a high Seebeck coefficient in both *n*- and *p*- type variants [15]. However, this prediction is yet to be tested experimentally.

In the search for new thermoelectric materials, we have investigated filled skutterudites based on the isoelectronic ternary phase $Fe_2Ni_2Sb_{12}$. In particular, we investigate the effect on thermoelectric and magnetic properties of varying degrees of filling through preparation of the new series of quaternary phases, $Yb_xFe_2Ni_2Sb_{12}$ ($0 \leq x \leq 0.4$).

2. Experimental

The skutterudites $Yb_xFe_2Ni_2Sb_{12}$ ($0 \leq x \leq 0.4$) were prepared by mixing stoichiometric quantities of the elements Fe (Alfa, 99.9%), Ni (Aldrich, 99.99%), Sb (Aldrich, 99.999%) and Yb (Aldrich, 99.9%). The reagents were loaded into glassy carbon crucibles in an Ar-filled glove box. The crucibles were loaded into fused silica tubes under an Ar atmosphere before transferring to a vacuum line. The tubes were then evacuated ($< 10^{-4}$ Torr) and sealed. The mixtures were heated for 12 hours at 1173 K, quenched in cold water and annealed at 873 K for 3 days. The tubes were opened in air and the solids finely ground before annealing in evacuated fused silica tubes at 873 K for 3 days.

The air-stable polycrystalline samples were characterised using a Bruker D8 Advance powder diffractometer, operating with germanium-monochromated Cu $K_{\alpha 1}$ radiation (λ = 1.5406 Å) and a LynxEye linear detector. The samples were loaded on zero-background holders and data were collected over the angular range $10 \leq 2\theta/^{\circ} \leq 120$ with a step of 0.0092°

in detector position and counting times between 1.2 and 1.8 s at each step, depending on the identity of the sample. Time-of-flight (TOF) neutron diffraction data for the parent phase $Fe_2Ni_2Sb_{12}$ were collected using the HRPD diffractometer at the ISIS Facility, Rutherford Appleton Laboratory, UK. The $Fe_2Ni_2Sb_{12}$ sample was sealed into an evacuated low-boron content silica tube and data were collected at 298 K. Initial data manipulation and reduction was carried out using the Mantid [16] software package. Neutron diffraction data from the backscattering and the 90^o detector banks were summed, normalised and used simultaneously in Rietveld refinement, which was carried out using the GSAS package [17].

Thermoelectric measurements were performed on hot-pressed pellets of $Yb_xFe_2Ni_2Sb_{12}$ (823 K, 60 MPa, 30 minutes, N_2 atmosphere). The densities of the resulting pellets correspond to *ca.* 95% of the crystallographic density. Rectangular blocks with approximate dimensions of 2 x 2 x 10 mm were cut from the pellets. Electrical resistivity measurements were performed using the four-probe DC method. Owing to the low resistance of the samples, measurements were made using a constant current power supply and a nanovoltmeter. Four 50 μm silver wires were attached to the block using colloidal silver paint and connections were made to a TT*i* QL564P power supply and a Keithley 2182 nanovoltmeter. The sample stick was mounted in an Oxford Instruments CF1200 cryostat connected to an ITC502 temperature controller and data were collected over the temperature range $80 \leq T / K \leq 360$ in 20 K steps. Seebeck coefficient measurements were performed over the temperature range $100 \leq T / K \leq 350$ in 5 K steps. The samples were mounted on a stick designed and built in-house, which includes a small heater located close to one end of the sample, thus allowing a temperature gradient to be applied to the sample. Two 50 μm copper wires were attached to the ends of the sample, and connections were made to a Keithley 2182 nanovoltmeter. Two Au:0.07%Fe vs. chromel thermocouples were placed in contact with the sample at the hot and cold ends, and connected to an ITC503 temperature controller (Oxford Instruments). The sample stick was placed in an Oxford Instruments CF1200 cryostat connected to an ITC502 temperature controller. The Seebeck coefficient, at a given temperature, was determined by

sweeping a temperature gradient, ΔT, of up to 5K and measuring the corresponding thermal voltage, ΔV [18]. The Seebeck coefficient was determined by extracting the gradient from a plot of ΔV vs. ΔT by least-squares fitting of the straight line. Thermal diffusivity measurements were carried out over the temperature range $373 \leq T/\mathrm{K} \leq 623$ in steps of 50 K using an Anter Flashline 3000 instrument. Measurements were made on 2 mm thick, 13 mm diameter pellets of *ca.* 95% of theoretical density. This instrument determines both the thermal diffusivity (α) and the heat capacity (C_p) of the sample, and the thermal conductivity (κ) is calculated from the relationship: $\kappa = \alpha C_p \rho$, where ρ is the sample density. For the determination of the heat capacity, side-by-side testing of a reference material, PyroceramTM 9606, of known heat capacity, was carried out. The procedure used for the determination of the heat capacity is described in detail in references [19] and [20].

Magnetic measurements were performed using a SQUID magnetometer (Quantum Design, MPMS XL). Data were collected over the temperature range $2 \leq T/\mathrm{K} \leq 300$ both after cooling in zero applied field (ZFC) and after cooling in the measuring field (FC) of 1000 G. The thermal stability of the samples at elevated temperatures was investigated with a DuPont 951 thermogravimetric analyser. The samples (*ca.* 30 mg each) were loaded into silica crucibles and heated at a rate of 2 K min^{-1} up to 1073 K under a 60 mL min^{-1} flow of air.

3. Results and Discussion

Rietveld refinements for $Fe_2Ni_2Sb_{12}$ were carried out using TOF powder diffraction data. The initial structural model was that proposed by Kjekshus and Rakke [21]. Analysis of neutron diffraction data indicates that this material crystallizes in the cubic space group $Im\bar{3}$. No superstructure reflections were observed in the neutron diffraction data, consistent with complete disorder of the transition-metal cations over the octahedral sites. This is in accord with previous observations on the Ce-filled skutterudites $Ce_\delta Fe_{4-x}Ni_xSb_{12}$ ($0.06 \leq \delta = (4 -$

$2x)/3 \leq 0.72$) [22]. Details of the neutron refinement are presented as Supplementary Information.

Rietveld refinements for $Yb_xFe_2Ni_2Sb_{12}$ were performed using powder X-ray diffraction data. A representative refinement for $Yb_{0.4}Fe_2Ni_2Sb_{12}$ is shown in Figure 2. All other profiles can be found in the Supplementary Information. Table 1 summarizes the refined parameters from the Rietveld analysis for $Yb_xFe_2Ni_2Sb_{12}$. In all refinements, the site occupancy factors of Fe and Ni atoms were constrained to their nominal values. The lattice parameters expand almost linearly with increasing Yb content (Figure 3). Selected bond lengths and angles are presented as Supplementary Information. The degree of Yb filling has little effect on the Sb – Fe/Ni – Sb distances within the $(Fe/Ni)Sb_6$ octahedra or on the Fe/Ni – Sb – Fe/Ni angles between the vertex-sharing octahedra. The ratio of the long to short Sb – Sb distances within the four-membered rings decreases slightly from 1.06 in the unfilled skutterudite to 1.04 beyond $x = 0.2$, indicating that the four-membered rings are becoming more square. The approach to square rings with increasing filling fraction appears to a general phenomenon in skutterudites [23]. The other interatomic distances show a slight increase with increasing Yb content.

The Rietveld analysis also indicates that the samples contain small amounts of Sb and/or Yb_2O_3 impurities. For higher nominal Yb contents, the amount of Yb_2O_3 impurity increases significantly, suggesting that the actual Yb content of the skutterudites is likely to be somewhat lower than indicated by the initial reaction stoichiometry. However, due to the strong correlation between the thermal displacement parameter, U_{iso}(Yb), and the site occupation factor, SOF(Yb), the latter could not be refined reliably with the Rietveld method.

The electrical resistivity of $Fe_2Ni_2Sb_{12}$ decreases with increasing temperature, consistent with semiconducting behaviour (Figure 4). However, the temperature dependence does not follow a simple Arrhenius-type behaviour. The electrical resistivity of the filled skutterudites is low and increases with increasing temperature: behaviour that would be expected for a metal. With increasing Yb content the resistivity at a given temperature falls which may be

attributed to an increasing charge carrier concentration. All compounds exhibit a negative Seebeck coefficient, indicating that electrons are the dominant charge carriers. $S(T)$ exhibits an almost linear dependence on temperature. The absolute value of the Seebeck coefficient increases with Yb content, reaching a maximum for $Yb_{0.15}Fe_2Ni_2Sb_{12}$, before decreasing at higher levels of Yb incorporation (Table 2). Such parabolic-like dependence of the Seebeck coefficient with the degree of filling has been previously found in $(Ba_{0.5}Yb_{0.5})_yCo_4Sb_{12}$ [24], and may reflect changes in the density of states as the position of the Fermi level changes on filling the skutterudite. The same parabolic-like dependence is observed for the magnitude of the slope of $S(T)$. The combination of a metal-like temperature dependence of both the resistivity and Seebeck coefficient, together with the relatively large absolute values of the latter, indicate that these materials are degenerate semiconductors. Further support for this view is provided by applying the equation of Zhang *et al*. [24] to estimate the charge carrier density, n. The Seebeck coefficient data presented here lead to values of n in the range 10^{20} - 10^{21} cm^{-3}, typical of those of heavily-doped semiconductors.

In agreement with previous literature reports [25], the thermal conductivity of $Fe_2Ni_2Sb_{12}$ (Table 2) is significantly lower than that of Co_4Sb_{12} ($\approx$ 9 W m^{-1} K^{-1} at 350 K). It has been suggested that mass defect scattering alone, cannot account for the reduction in thermal conductivity with changing framework composition in this pair of isoelectronic skutterudites, and that additional mechanisms, such as mixed valency, must be involved [25]. In $Yb_xFe_2Ni_2Sb_{12}$, partial occupancy of the framework voids with Yb leads to a further reduction of the thermal conductivity, by up to 35%. By applying the Wiedemann-Franz law ($\kappa_e = LT/\rho$ where L = 2.44 10^{-8} W Ω K^{-2}), the electronic contribution to the thermal conductivity at 350 K is estimated to be relatively small and to increase with increasing Yb content: rising from 3% of the total thermal conductivity for $Fe_2Ni_2Sb_{12}$ to 21% for $Yb_{0.4}Fe_2Ni_2Sb_{12}$. Thus, the lattice vibrations are the main contributors to the thermal conductivity and κ_{latt} in the partially filled skutterudites is approximately half the value of that in $Fe_2Ni_2Sb_{12}$. It has previously been suggested that this reduction arises primarily from localised (rattling) vibrational modes of the

filler atom [9]. However, given the incomplete filling of the void sites, it is likely that mass fluctuation scattering between empty and filled sites, plays a role in reducing the thermal conductivity [26].

Despite the low thermal conductivity, the power factors (S^2/ρ) and ultimately the *ZT* values of the title compounds are relatively low. This may be traced to the higher resistivity and lower Seebeck coefficient of the materials reported here compared with those for analogous cobalt containing phases. For example, the values for $Yb_{0.19}Co_4Sb_{12}$ at 350 K are 0.7 mΩ cm and -150 μV K^{-1} respectively, yielding $ZT \approx 0.25$ [27]. One possible explanation for the high electrical resistivity could be the reduced mobility of the charge carriers in the Fe/Ni skutterudites. Similar findings have been reported for the double-filled $(Pr,Nd)_{0.08}Fe_2Ni_2Sb_{12}$ skutterudite [13], which also shows lower *ZT* values than $(Pr,Nd)_{0.08}Co_4Sb_{12}$ [13] at temperatures below 700 K. Higher figures of merit have been obtained in the skutterudites $(Pr,Nd)_y(Fe_{1-x}Ni_x)_4Sb_{12}$ [13] and $(Ce,Yb)_y(Fe_{1-x}Ni_x)_4Sb_{12}$ [14] by controlling the Fe/Ni ratio, which provides an additional degree of freedom in optimising the charge carrier density.

The skutterudites show paramagnetic behaviour over the temperature range $2 \leq T/K \leq 300$ (Figure 5). ZFC and FC data overlie each other throughout the temperature range investigated. With the exception of $Yb_{0.2}Fe_2Ni_2Sb_{12}$ all compounds follow the Curie-Weiss law at higher temperatures. The unfilled skutterudite shows Curie-Weiss behaviour over a more restricted range of temperatures than for the quaternary phases. Derived magnetic parameters are presented in Table 3. All materials exhibit large negative Weiss constants, indicating that the dominant exchange interactions are antiferromagnetic in origin. For the unfilled skutterudite, $Fe_2Ni_2Sb_{12}$, assuming that both cations are formally trivalent with low-spin electron configurations leads to a theoretical Curie constant of 1.5 cm^3 K mol^{-1}. This compares favourably with the value of 1.67(2) cm^3 K mol^{-1} determined experimentally. Previously reported magnetic measurements on $Co_{1-x}Fe_xSb_3$ are also consistent with a low-spin d^5 configuration for iron [28]. Our magnetic data also appear to refute the suggestion by

Fleurial *et al.* [25] of formal oxidation states of Fe^{2+} and Ni^{4+}, as the low-spin d^6 configurations of these ions would lead to diamagnetic behaviour. Interpretation of the magnetic properties of the filled skutterudites is complicated by the presence of the paramagnetic impurity phase, Yb_2O_3. However, some general conclusions may be drawn. At the lowest level of Yb incorporation, the experimentally determined effective magnetic moment per cation is in good agreement with μ_{th}, calculated on the basis of complete transfer of three electrons per Yb^{3+} to a framework of Fe^{3+}/Ni^{3+}. With higher degrees of Yb incorporation the effective magnetic moment per cation increases, due to both the large contribution from Yb^{3+} (μ_{eff}^2 = 20.6 μ_B) and electron transfer to the framework, which increases the value of the electron spin associated with Ni^{3+}. Discrepancies between the observed and calculated effective magnetic moments may be due to a number of factors, in addition to the presence of paramagnetic Yb_2O_3 impurities, including spin-orbit coupling effects [29] and a mixed or intermediate valence of the cations. It has been suggested on the basis of X-ray absorption spectroscopy experiments [14], that the Yb valence state in Yb-filled skutterudites decreases progressively from the trivalent to divalent state with increasing Yb content, whilst in $YbFe_4Sb_{12}$ [30] all Yb is in the divalent state.

Thermal stability studies were carried out for $Fe_2Ni_2Sb_{12}$, $Yb_{0.2}Fe_2Ni_2Sb_{12}$ and $Yb_{0.4}Fe_2Ni_2Sb_{12}$. The onset of oxidation, as evidenced by the sample beginning to gain weight, occurs at *ca*. 550 K for all three compounds (Figure 6). The decomposition products were identified as mixtures of SbO_2, $FeSbO_4$ and $NiSb_2O_6$ by powder X-ray diffraction. The experimental weight gain (*ca.* 23 % to 28 %) is slightly lower than the expected value of 30.3% for the complete conversion of the skutterudites to this mixture of oxides. The thermal stability of $Yb_xFe_2Ni_2Sb_{12}$ is significantly lower than that of $Yb_{0.2}Co_4Sb_{12}$ (Fig. S9 in the Supporting information), the oxidation of which occurs above *ca.* 650 K. The instability of the skutterudites with respect to oxidation at elevated temperatures, presents a barrier to their implementation in practical devices. This suggests that in a device, such materials would

require protection against oxidation, through the deposition of protective barrier layers [31, 32].

4. Conclusions

The Yb-filled compounds $Yb_xFe_2Ni_2Sb_{12}$ ($0 \leq x \leq 0.4$) represent new members of the filled skutterudite family and behave as *n*-type, degenerate semiconductors. The Yb filling affects the thermal and electrical transport properties. The optimum filler content, with respect to the thermoelectric performance at 350 K, is found for $Yb_{0.15}Fe_2Ni_2Sb_{12}$. Although the title compounds contain less costly elements than the analogous filled cobalt antimonides and also exhibit a significantly lower thermal conductivity than their cobalt congeners, their thermoelectric performance is somewhat lower, as exemplified by comparing the values $ZT(Yb_{0.15}Fe_2Ni_2Sb_{12}) = 0.064$ and $ZT(Yb_{0.19}Co_4Sb_{12}) \approx 0.25$ at 350 K. However, further optimisation of the thermoelectric response of filled ternary skutterudites may be possible through tuning of the Fe:Ni ratio.

Acknowledgements

The authors wish to thank the UK EPSRC for financial support (EP/H050396) and the STFC for access to neutron scattering facilities.

Supplementary Information

Rietveld plots from neutron and X-ray diffraction data for $Yb_xFe_2Ni_2Sb_{12}$, table of Rietveld refinement parameters from neutron diffraction data for $Fe_2Ni_2Sb_{12}$, tables of selected bond lengths and angles for $Yb_xFe_2Ni_2Sb_{12}$, reciprocal magnetic susceptibility data for $Yb_xFe_2Ni_2Sb_{12}$, and the thermogravimetric data for $Yb_{0.2}Co_4Sb_{12}$ are available.

References

[1] R.H. Mitchell, Perovskites: Modern and Ancient, Almaz Press, Ontario, Canada, 2002.

[2] A.M. Glazer, Acta Crystallogr. Sect. B 28 (1972) 3384-3392.

[3] C. Uher in: M.G. Kanatzidis, T.P. Hogan, S.D. Mahanti (Eds.), Chemistry, Physics and Materials Science of Thermoelectric Materials: Beyond Bismuth Telluride, Springer, 2003, pp. 121–146.

[4] W. Jeitschko, D. Braun, Acta Crystallogr. Sect. B 33 (1977) 3401–3406.

[5] G.S. Nolas, D.T. Morelli, T.M. Tritt, Annu. Rev. Mater. 29 (1999) 89–116.

[6] A. Shevelkov, Russ. Chem. Rev. 77 (2008) 1–19.

[7] J. Sootsman, D. Chung, M. Kanatzidis, Angew. Chem. Int. Ed. 48 (2009) 8616–8639.

[8] G. Slack in: D.M. Rowe (Ed.), CRC Handbook of Thermoelectrics, CRC Press, 1995, p. 407.

[9] V. Keppens, D. Mandrus, B.C. Sales, B.C. Chakoumakos, P. Dai, R. Coldea, M.B. Maple, D.A. Gajewski, E.J. Freeman, S. Bennington, Nature 395 (1998) 876–878.

[10] X. Tang, Q. Zhang, L. Chen, T. Goto, T. Hirai, J. Appl. Phys. 97 (2005) 093712.

[11] B.C. Sales, D. Mandrus, B.C. Chakoumakos, V. Keppens, J.R Thompson, Phys. Rev B 56 (1997) 15081–15089.

[12] E. Bauer, S. Berger, G. Hilscher, H. Michor, C. Paul, M. Reissner, W. Steiner, A. Grytsiv, P. Rogl, 22nd International Conference on Thermoelectrics, Proceedings ICT '03 (2003) 89–92.

[13] G. Rogl, A. Grytsiv, E. Bauer, P. Rogl, M. Zehetbauer, Intermetallics 18 (2010) 57–64.

[14] D. Bérardan, E. Alleno, C. Godart, O. Rouleaum, J. Rodriguez-Carvajal, Mat. Res. Bull. 40 (2005) 537–551.

[15] D. J. Singh, M.-H. Du, Phys. Rev. B 82 (2010) 075115.

[16] Details of the Mantid High-Performance Computing Project may be found at http://www.mantidproject.org

[17] A.C. Larson, R.B. von Dreele, General Structure Analysis System, Los Alamos Laboratory, [Report LAUR 85-748], 1994.

[18] G.R. Caskey, D.J. Sellmeyer, L.G. Rubin, Rev. Sci. Instrum. 40 (1969) 1280–1282.

[19] P.S. Gaal, S.P. Apostolescu, US patent No. US 6,375,349 (2002).

[20] M.-A. Thermitus, P.S. Gaal, Proceedings of the 24th International Thermal Conductivity Conference, Eds. C. Uher and D. Morelli, Technomic Publishing Co., Lancaster, p. 340 (2000).

[21] A. Kjekshus, T. Rakke, Acta Chemica Scandinavica, Series A - Physical and Inorganic Chemistry 28 (1974) 99–103.

[22] L. Chapon, L. Girard, A. Haidoax, R.I. Smith, D. Savot, J. Phys: Condens. Matter 17 (2005) 3525–3535.

[23] B.C. Chakoumakos, B.C. Sales, J. Alloys Comp. 407 (2006) 87–93.

[24] L. Zhang, A. Grytsiv, P. Rogl. E. Bauer, M. Zehetbauer, J. Phys. D: Appl. Phys. 42 (2009) 225405.

[25] J.-P. Fleurial, T. Caillat, A. Borshchevsky, 16th International Conference on Thermoelectrics (1997) 1–11.

[26] G.P. Meisner, D.T. Morelli, S.Hu, J. Yang, C. Uher, Phys. Rev. Lett., 80 (1998) 3551-3554.

[27] G.S. Nolas, M. Kaeser, R.T. Littleton, T.M. Tritt, Appl. Phys. Lett. 77 (2000) 1855–1857.

[28] J. Yang, G.P. Meisner, D.T. Morelli, C. Uher, Phys. Rev. B, 63 (2000) 014410.

[29] M.E. Danebrock, C.B.H. Evers, W. Jeitschko, J. Phys. Chem. Solids 57 (1996) 381–387.

[30] W. Schnelle, A. Leithe-Jasper, M. Schmidt, H. Rosner, H. Borrmann, U. Burkhardt, J.A. Mydosh, Y. Grin, Phys. Rev. B 72 (2005) 020402.

[31] M.S. El-Genk, H.H. Saber, T. Caillat, J. Sakamoto, Energy Conversion and Management 47 (2006) 174–200.

[32] P. Wei, W.-Y. Zhao, C.-L. Dong, B. Ma, Q.-J. Zhang, Journal of Electronic Materials 39 (2010) 1803–1808.

Table 1 Rietveld refinement data using X-ray diffraction data for $Yb_xFe_2Ni_2Sb_{12}$ (Space group $Im\bar{3}$).

Nominal composition	$Fe_2Ni_2Sb_{12}$	$Yb_{0.15}Fe_2Ni_2Sb_{12}$	$Yb_{0.2}Fe_2Ni_2Sb_{12}$	$Yb_{0.3}Fe_2Ni_2Sb_{12}$	$Yb_{0.4}Fe_2Ni_2Sb_{12}$
Lattice parameter, a / Å	9.08865(2)	9.09392(7)	9.09875(4)	9.10256(7)	9.10699(6)
y(Sb)	0.33368(9)	0.33514(13)	0.33617(11)	0.33541(12)	0.33615(9)
z(Sb)	0.15633(10)	0.15740(13)	0.15815(12)	0.15754(13)	0.15819(9)
U_{iso}(Sb) / Å^2	0.0091(3)	0.0109(5)	0.0088(2)	0.0062(6)	0.0027(2)
U_{iso}(Fe/Ni) / Å^2	0.0044(7)	0.0122(11)	0.0105(10)	0.0033(11)	0.0006(7)
SOF(Yb)	-	0.15	0.2	0.3	0.4
U_{iso}(Yb) / Å^2	-	0.186(21)	0.069(7)	0.051(5)	0.109(4)
Sb impurity (wt.%)	2.9(1)	0	2.1(1)	0	3.5(1)
Yb_2O_3 impurity (wt.%)	0	0.95(5)	0	2.8(1)	2.7(1)
χ^2 (%)	1.78	1.29	1.53	1.84	1.90
R_{wp} (%)	10.0	11.1	9.29	10.3	8.5

Sb on 24*g*, (*0*,*y*,*z*); Fe/Ni on 8*c* (¼,¼,¼); Yb on 2*a*, (*0*,*0*,*0*)

Table 2 Thermoelectric properties for $Yb_xFe_2Ni_2Sb_{12}$ at 350 K.

Compound	Electrical resistivity, ρ / mΩ cm	Seebeck coefficient, S / μV K^{-1}	Power factor, $S^2 \rho^{-1}$ / mW m^{-1} K^{-2}	Thermal conductivity[a], κ / W m^{-1} K^{-1}	ZT
$Fe_2Ni_2Sb_{12}$	7.53	-38	0.019	3.9	0.0017
$Yb_{0.15}Fe_2Ni_2Sb_{12}$	4.05	-133	0.437	2.4	0.064
$Yb_{0.2}Fe_2Ni_2Sb_{12}$	2.56	-85	0.282	2.1	0.047
$Yb_{0.3}Fe_2Ni_2Sb_{12}$	2.14	-81	0.307	2.5	0.043
$Yb_{0.4}Fe_2Ni_2Sb_{12}$	1.58	-60	0.228	2.5	0.032

[a] values of κ at 350 K were obtained by extrapolation from measured values at 373 K

Table 3 Parameters derived from magnetic susceptibility data for $Yb_xFe_2Ni_2Sb_{12}$.

Compound	Temperature range / K	C / cm^3 K mol^{-1}	Θ / K	μ_{exp} per cation	μ_{th} per cation
$Fe_2Ni_2Sb_{12}$	120 – 300	1.67(2)	-822(5)	1.83(1)	1.73
$Yb_{0.15}Fe_2Ni_2Sb_{12}$	40 – 300	1.41(3)	-276(6)	1.65(2)	2.02
$Yb_{0.3}Fe_2Ni_2Sb_{12}$	40 – 300	5.67(1)	-309(35)	3.25(1)	2.27
$Yb_{0.4}Fe_2Ni_2Sb_{12}$	40 – 300	4.63(1)	-441(9)	2.90(1)	2.42

Figure Captions

Figure 1. The crystal structure of the filled skutterudite $Yb_xFe_2Ni_2Sb_{12}$. Key: Sb, small open circles; Yb, large shaded circles. Disordered Fe/Ni atoms reside in the center of the shaded octahedra.

Figure 2. Final observed (crosses), calculated (solid line) and difference (lower full line) profiles from Rietveld refinement using X-ray powder diffraction data for $Yb_{0.4}Fe_2Ni_2Sb_{12}$. Upper, middle and lower markers represent the peak positions for $Yb_{0.4}Fe_2Ni_2Sb_{12}$, Yb_2O_3 and Sb, respectively.

Figure 3. The lattice parameter of of $Yb_xFe_2Ni_2Sb_{12}$ as a function of the nominal Yb content – error bars lie within the points.

Figure 4. Thermoelectric properties for the $Yb_xFe_2Ni_2Sb_{12}$ skutterudites: (a) electrical resistivity on a logarithmic scale; (b) Seebeck coefficient; (c) power factor and (d) thermal conductivity.

Figure 5. Molar magnetic susceptibility data for $Yb_xFe_2Ni_2Sb_{12}$.

Figure 6. Thermogravimetric data for $Fe_2Ni_2Sb_{12}$, $Yb_{0.2}Fe_2Ni_2Sb_{12}$, $Yb_{0.4}Fe_2Ni_2Sb_{12}$.

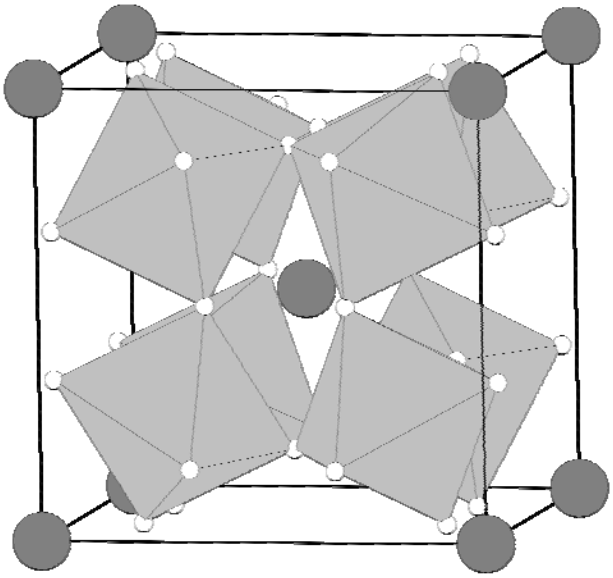

Figure 1

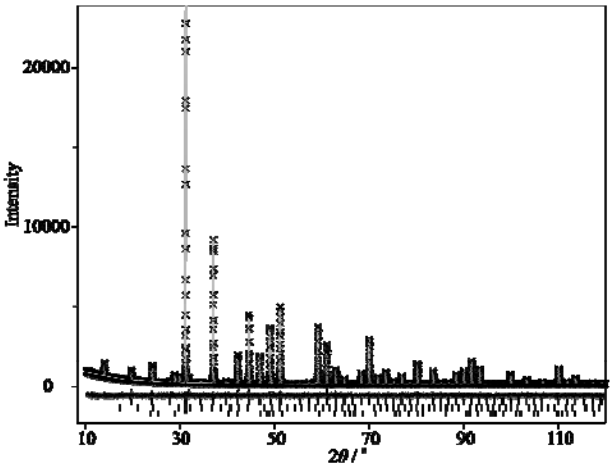

Figure 2

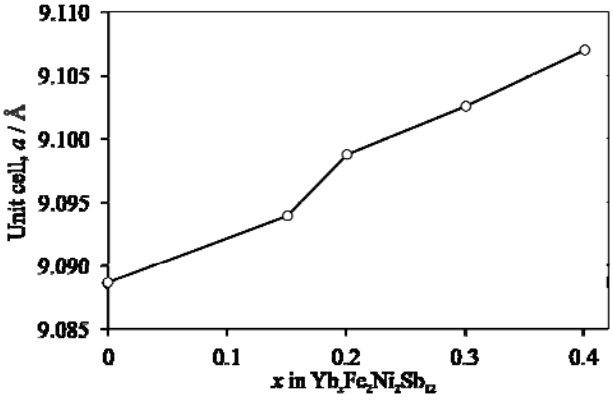

Figure 3

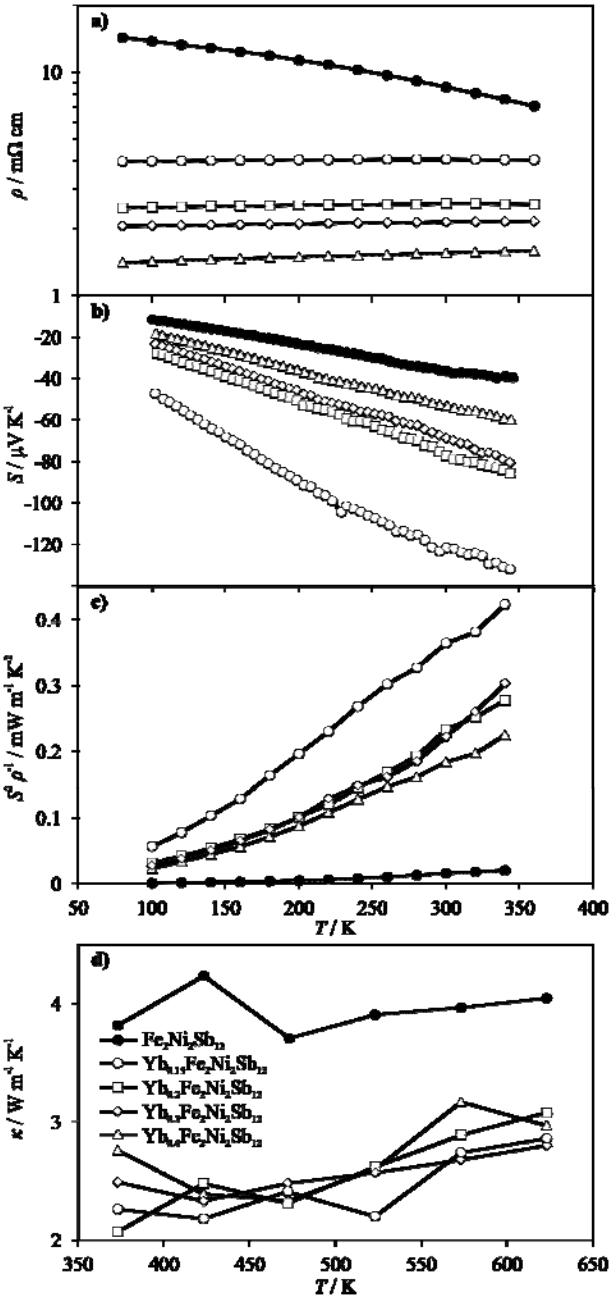

Figure 4

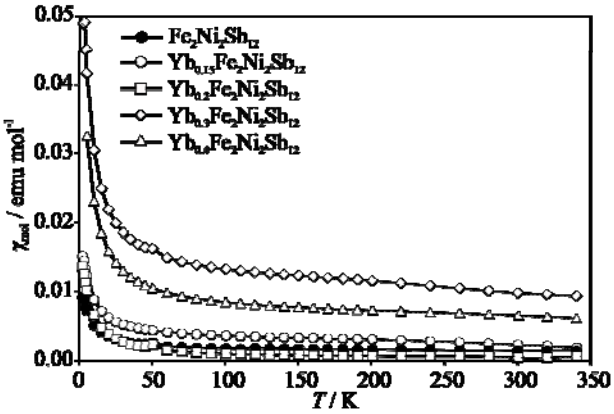

Figure 5

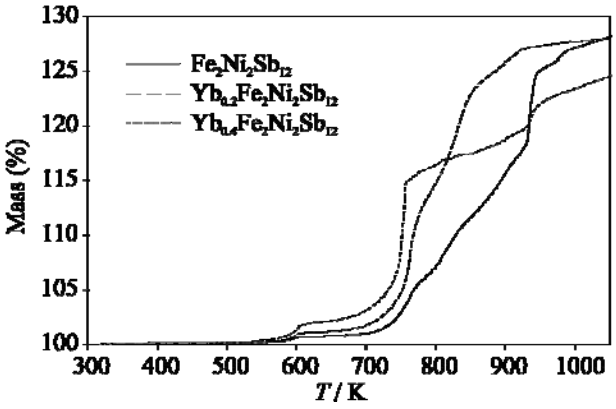
130
125
120
115
110
105
100
Mass (%)
300
400
500
600
700
800
900
1000
T / K
Fe2Ni2Sb12
Yb0.2Fe2Ni2Sb12
Yb0.4Fe2Ni2Sb12

Figure 6